Manuscript prepared for J. Name
with version 4.2 of the LaTeX class copernicus.cls.
Date: 15 July 2014

Constraining the N_2O_5 UV absorption cross-section from spectroscopic trace gas measurements in the tropical mid-stratosphere

L. Kritten[1,*], A. Butz[2,*], M. P. Chipperfield[3], M. Dorf[4,*], S. Dhomse[3], R. Hossaini[3], H. Oelhaf[2], C. Prados-Roman[5,*], G. Wetzel[2], and K. Pfeilsticker[6]

[1]Institute for Space Sciences (WEW), Free University Berlin, Berlin, Germany
[2]Karlsruhe Institute of Technology, IMK-ASF, Karlsruhe, Germany
[3]Institute for Climate and Atmospheric Science, School of Earth and Environment, University of Leeds, Leeds, UK
[4]Max-Planck-Institute for Chemistry, Mainz, Germany
[5]Atmospheric Chemistry and Climate Group, Institute of Physical Chemistry Rocasolano (CSIC), Madrid, Spain
[6]Institute of Environmental Physics (IUP), University of Heidelberg, Heidelberg, Germany
[*]formerly at: Institute of Environmental Physics (IUP), University of Heidelberg, Heidelberg, Germany

Abstract. The absorption cross-section of N_2O_5, $\sigma_{N_2O_5}(\lambda,T)$, which is known from laboratory measurements with the uncertainty of a factor of 2 (table 4-2 in JPL-2011 (Sander et al., 2011)), was investigated by balloon-borne observations of the relevant trace gases in the tropical mid-stratosphere. The method relies on the observation of the diurnal variation of NO_2 by limb scanning DOAS measurements (Weidner et al. (2005),Kritten et al. (2010)), supported by detailed photochemical modelling of NO_y (NO_x(=NO+NO_2)+NO_3+2N_2O_5+$ClONO_2$+HO_2NO_2 +$BrONO_2$+HNO_3) photochemistry and a non-linear least square fitting of the model result to the NO_2 observations. Simulations are initialised with O_3 measured by direct sun observations, the NO_y partitioning from MIPAS-B (Michelson Interferometer for Passive Atmospheric Sounding-Balloon) observations in similar air masses at nighttime, and all other relevant species from simulations of the SLIMCAT chemical transport model (CTM). Best agreement between the simulated and observed diurnal increase of NO_2 is found if the $\sigma_{N_2O_5}(\lambda,T)$ is scaled by a factor of 1.6 ± 0.8 in the UV-C (200 - 260 nm) and by a factor of 0.9 ± 0.26 in the UV-B/A (260 - 350 nm), compared to current recommendations. In consequence, at 30 km altitude, the N_2O_5 lifetime against photolysis becomes a factor of 0.77 shorter at solar zenith angle (SZA) of 30° than using the recommended $\sigma_{N2O5}(\lambda,T)$, and stays more or less constant at SZAs of 60°. Our scaled N_2O_5 photolysis frequency slightly reduces the lifetime (0.2 - 0.6%) of ozone in the tropical mid- and upper stratosphere, but not to an extent to be important for global ozone.

Keywords. Stratosphere photochemistry, limb scanning, cross-section of N_2O_5, UV/vis spectroscopy, photochemical modelling

Correspondence to: L. Kritten (lkritten@wew.fu-berlin.de)

1 Introduction

The NO_x ozone loss cycle dominates catalytic ozone loss in the mid-stratosphere (25 - 45 km) and the ozone production via coupling with the HOx cycle below about 20 km (e.g., Brasseur and Solomon (2005)). In future it is predicted to increase further in relevance, since the emissions of its major precursor N_2O are increasing, while emissions of other ozone-depleting substances (ODS) are decreasing (Ravishankara et al., 2009). Signs that this is already happening come from the recent analysis of ozone vertical profile time series from SCIAMACHY satellite instrument limb measurements (Gebhardt et al., 2013), since they show a negative trend of ozone in the tropics above 30 km and a positive trend below. The explanation most favoured by the authors is due to NO_x photochemistry, which catalytically destroys stratospheric ozone (e.g., Crutzen (1970), and Johnston (1971)) (see below).

A second motivation to study the photolysis frequency of N_2O_5 comes through the finding of often overpredicted N_2O_5, most strikingly found in comparison studies of MIPAS/ENVISAT N_2O_5 data with predictions of a suite of photochemical transport models for the lower and middle stratosphere ($p > 10$ mbar) (e.g., Brühl et al. (2007), and Funke et al. (2011)). Unpublished SLIMCAT sensitivity runs are indicating that a more rapid photolysis of N_2O_5 (up to factor of 2) than supported by $\sigma_{N2O5}(\lambda,T)$ from JPL-2011 (Sander et al., 2011) would largely help to close this gap.

In the context of ozone loss, most crucial is how fast major nighttime NO_y species (e.g., HNO_3, N_2O_5, and $ClONO_2$) are recycled into ozone destroying NO_x at daytime. Catalytic ozone destruction by the NO_x photochemistry occurs through the following reactions

$$NO + O_3 \rightarrow NO_2 + O_2 \quad \text{(R1)}$$
$$O + NO_2 \rightarrow NO + O_2 \quad \text{(R2)}$$
$$net: O + O_3 \rightarrow 2O_2 \quad \text{(R3)}$$

The primary source of stratospheric NO_x is the photolytic destruction of N_2O (R4, R5, and R6).

$$N_2O + O(^1D) \rightarrow 2 \cdot NO \quad \text{(R4)}$$
$$\rightarrow N_2 + O_2 \quad \text{(R5)}$$
$$N_2O + h\nu \rightarrow N_2 + O(^1D) \quad \text{(R6)}$$

N_2O is mostly emitted by biological and combustion processes at the surface, but their N_2O emissions are not regulated by the Montreal Protocol (e.g., IPCC (2007), and WMO (2011)). Accordingly, atmospheric N_2O concentrations are presently increasing with a rate of 0.75 ppb per year (Park et al. (2012) and WMO Press Release (No. 934)).

Four major processes determine the effect of N_2O on stratospheric ozone:

(1) The competition of the N_2O destruction processes R4 leading to NO_x production (about 7% for any N_2O destroyed) and reactions R5 and R6 only destroying N_2O without producing NO_x.

(2) The sink reactions R7 and R8

$$NO + h\nu \rightarrow N(^4S) + O \quad \text{(R7)}$$

followed by

$$NO + N \rightarrow N_2 + O \quad \text{(R8)}$$

are known to destroy NO_x in the middle and upper stratosphere.

(3) Further it is well known that during daytime reaction R1 and the photolysis of NO_2

$$NO_2 + h\nu \rightarrow NO + O \quad \text{(R9)}$$

readily establish a steady state between NO and NO_2, thus determining the amount of NO_2 available for the odd-oxygen-destroying reaction R2.

(4) The fourth major factor controlling the ozone depletion potential of NO_x, and thus of N_2O, are reactions leading to the so-called NO_y reservoir species (NO_y = NO_x+NO_3+2N_2O_5+$ClONO_2$+HO_2NO_2 +$BrONO_2$+HNO_3) of which all except HNO_3 are important for the diurnal variation of NO_x, and thus NO_x-mediated ozone loss. Among them N_2O_5 is most important in the tropical mid-stratosphere (as shown in Figure 1). First NO_3 has to be formed by the reaction

$$NO_2 + O_3 \rightarrow NO_3 \quad \text{(R10)}$$

then N_2O_5 can be formed by the termolecular reaction

$$NO_2 + NO_3 + M \rightarrow N_2O_5 + M \quad \text{(R11)}$$

and destroyed by thermal decomposition R12, photolysis R13, and the heterogeneous reaction R14, where aerosols are abundant, i.e. in the lower stratosphere (Brasseur and Solomon, 2005).

$$N_2O_5 + M \rightarrow NO_2 + NO_3 + M \quad \text{(R12)}$$
$$N_2O_5 + h\nu \rightarrow NO_2 + NO_3 \quad \text{(R13)}$$
$$N_2O_5 + H_2O_{aq} \rightarrow 2HNO_3 \quad \text{(R14)}$$

R13 is particularly relevant for the daytime increase of NO_x in the tropical mid-stratosphere, since the product of photolysis rate $J_{N_2O_5}$ and concentration of N_2O_5 is the largest among the reservoir species under the given conditions (see Figure 1). The $J_{N_2O_5}$ is determined by the actinic flux $F(\lambda)$, the absorption cross-section of $J_{N_2O_5}$, $\sigma_{N_2O_5}(\lambda,T)$ and the quantum yield for photo-dissociation $\phi(\lambda)$ into the channels:

$$N_2O_5 + h\nu \rightarrow NO_2 + NO_3 \quad \text{(R15)}$$
$$\rightarrow NO_3 + NO + O(3P) \quad \text{(R16)}$$
$$\rightarrow NO_3 + NO_2* \quad \text{(R17)}$$

(Brasseur and Solomon, 2005). The photolyis rate $J_{N_2O_5}$ in each channel is then given by

$$J_{N_2O_5} = \int F(\lambda) \cdot \sigma_{N_2O_5}(\lambda,T) \cdot \phi(\lambda) \cdot d\lambda \quad (1)$$

The slightly temperature-dependent $\sigma_{N_2O_5}(\lambda,T)$ decreases from the extreme UV-C (λ = 200 nm) to the visible spectral range (λ = 400 nm) over 8 to 9 orders of magnitude (Figure 2). On the other hand the actinic flux $F(\lambda)$ strongly increases with wavelength resulting in two distinct maxima of the actinic spectrum in the mid- and upper stratosphere (i.e. in the UV-C and UV-B) (Figure 3), of which the shape depends on the solar zenith angle (SZA). The short wavelength maximum of the actinic spectrum is located around λ = 220 nm and the long wavelength maximum between λ = 280 and 320 nm.

In the laboratory, $\sigma_{N_2O_5}(\lambda,T)$ was first measured by Jones and Wulf (1937) and later by many others (see section 2.2). Current estimates of $\sigma_{N_2O_5}(\lambda,T)$ together with its uncertainties (a factor of 2) are reported in the JPL-2011 compendium (Table 4-2). However, to our knowledge $\sigma_{N_2O_5}(\lambda,T)$ has never been inferred from field observations.

Here balloon-borne measurements in the tropical mid-stratosphere of the diurnal variation of NO_2 (Kritten et al., 2010) are exploited to infer $\sigma_{N_2O_5}(\lambda,T)$ under stratospheric conditions. For the interpretation of the measured data with respect to $\sigma_{N_2O_5}(\lambda,T)$, a 1-D photochemical model is used. The model is initialised and further constrained by trace gas observations (O_3, and a suite of NO_y species) taken within the so-called tropical pipe over north-eastern Brazil during summer 2005. Further, an optimal estimation approach is used to minimise the quadratic difference of the measured from modelled concentration field of NO_2 as a function of

time and height. For this purpose $\sigma_{N_2O_5}(\lambda,T)$ is scaled by two free parameters (denoted by s_1 and s_2) in the extreme UV-C (200 - 258 nm) (denoted by w_1 wavelength range), and UV-B/A spectral range (260 - 420 nm) (denoted by w_2 wavelength range), respectively.

The paper is organised as follows. In section 2 the tools used in the study are described, including the NO_2 measurements, some details of the NO_y photochemical modelling as well as the mathematics to retrieve $\sigma_{N_2O_5}(\lambda,T)$. Section 3 reports on the results and discusses uncertainties. Section 4 addresses the implication of our findings for stratospheric N_2O_5 and global ozone. Section 5 concludes the study.

2 Measurements, photochemical modelling, and $\sigma_{\mathbf{N_2O_5}}(\lambda,\mathbf{T})$ retrieval

This section describes our approach to constrain $\sigma_{N_2O_5}(\lambda,T)$ from the NO_2 measurements in the tropical mid-stratosphere (Kritten et al., 2010) (section 2.1). Further the photochemical modelling including its initialisation by information gained from additional trace gas measurements in the tropical stratosphere and from simulations of the SLIMCAT CTM (section 2.2) is described. Finally the retrieval of the scaling parameters of $\sigma_{N_2O_5}(\lambda,T)$ for two wavelength intervals w_1 and w_2 (section 2.3) is discussed.

2.1 Measurements

For this study, time-dependent profiles of stratospheric NO_2 are used, which were measured over north-eastern Brazil (5.1° S, 43.6° W) on June 30, 2005 (see Figure 8 in Kritten et al. (2010)). During the balloon flight 187 limb spectra were recorded during 17 limb sequences, which covers 5:35 hours from local sunrise (7:30 LT) into the early afternoon (13:05 LT). The measured limb spectra were analyzed for differential slant column densities (DSCDs) using the DOAS (Differential Optical Absorption Spectroscopy) technique (e.g., Weidner et al. (2005), Kreycy et al. (2013) and Platt and Stutz (2008)). Prior to the inversion of the measured DSCDs into an NO_2 concentration height and time field, the radiative transfer for each measurement is modelled using the radiative transfer model (RTM) McArtim (Deutschmann et al., 2011). Further, the RT calculations are validated against measured limb radiances and inferred O_4 and O_3. The measured array of NO_2 DSCDs is then projected into a NO_2 concentration versus height and time field of equal altitude (h_i = 0.5 km) and time spacing (t_j = 30 min), using the optimal estimation technique (e.g., Rodgers (2000), and Kritten et al. (2010)). Due to decay of the NO_y reservoir species during daytime, at 33 km where the NO_2 profile peaks, NO_2 increases by roughly 60% during our observation. Our analysis is limited to SZAs $\leq 85°$ in order to reduce effects due to refraction which is not properly accounted for in the RTM McArtim (Deutschmann et al., 2011).

Major errors and shortcomings of our NO_2 measurements are the remaining pitch and azimuth angle oscillations of the balloon platform (see Figure 6 in Kritten et al. (2010)). While the former lead to a vertical jitter in the field of view, resulting in an up to $\pm 10\%$ uncertainty in the inferred NO_2 concentrations, the azimuth angle oscillations are more difficult to deal with. The latter is mainly due to the importance of polarisation (which is not yet considered in our RTM) of the scattered light from stratospheric limb measurements in the UV/visible wavelength range, mainly if during the course of the measurements the azimuthal scattering angle changes. Therefore, in order to remove any systematic errors due to the movement of the balloon gondola, the inferred NO_2 field is re-normalised using the inferred field of O_3. This is justified, by the constant O_3 concentration during the course of the measurement, and the similar optical depths at the wavelengths considered in the spectral analysis of O_3 and NO_2. For this purpose a weighting matrix is derived by dividing the retrieved O_3 concentration for each altitude (h_i) and time (t_j) step by the mean O_3 concentration of the whole balloon flight.

$$[NO_{2,corr}]_{i,j} = [NO_{2,retr}]_{i,j} \cdot \frac{[O_{3,mean}]_i}{[O_{3,retr}]_{i,j}} \qquad (2)$$

It is found that the re-normalisation alters the NO_2 field by 15% at most. Further on in the study, the renormalised NO_2 field (shown in the lower panel of Figure 4) is used, rather than the field inferred in Kritten et al. (2010) (see Figure 8 therein).

2.2 Modelling of the NO_y photochemical system

Since for the present study the calculation of the photolysis rates and the photochemical evolution is crucial, both deserve to be addressed. The photolysis rates are calculated by a module adopted from the SLIMCAT 3-D CTM (Bösch et al. (2003), Chipperfield (2006)) with updated molecular absorption cross-sections for N_2O_5 and HNO_3 (Sander et al., 2011). First, the actinic fluxes are calculated as recommended by Lary and Pyle (1991) and stored in a look-up table. Then, in order to scale the actinic fluxes to the actual atmospheric conditions, the calculated photolysis rates are interpolated to the actual pressure, temperature, SZA, and overhead ozone. For the latter an ozone profile is used, which was measured by balloon-borne solar occultation observations a few days prior to the NO_2 measurements (Butz et al., 2006). $J_{N_2O_5}$ skylight radiances were already validated in previous studies of our group (e.g., Bösch et al. (2003), Deutschmann et al. (2011)).

For calculation of $J_{N_2O_5}$, the $\sigma_{N_2O_5}(\lambda,T)$ based on the recommendation of the JPL-2011 compendium as shown in Figure 2) is used (Sander et al., 2011). $\sigma_{N_2O_5}(\lambda,T)$ ranges over about 9 orders of magnitude (from about 10^{-17} cm^2 at 200 nm to 10^{-26} cm^2 at 450 nm). The temperature dependence of $\sigma_{N_2O_5}(\lambda,T)$ is derived according to Harwood et al.

(1993). This only becomes significant at wavelengths greater than 280 nm, where $\sigma_{N_2O_5}(\lambda,T)$ decreases (decreasing with an increasing T-dependence for larger wavelengths).

The study of Oh et al. (1986) indicates that, besides NO_3, the primary photolysis products of N_2O_5 are a wavelength-dependent mixture of NO_2, NO_2^* and NO + O, where NO_2^* represents NO_2 in an excited electronic state (see reactions R15, R16 and R17). The measured quantum yield for the NO_3 production is close to unity. Since all product channels finally lead to the production of NO_x through fast reactions (within several 10th of seconds), and the equilibrium between NO and NO_2 is rapidly established in the sunlit stratosphere, the N_2O_5 photolysis is the time limiting factor for the NO_2 production. The combined uncertainties of the absorption cross-section and quantum yield cause $\sigma_{N_2O_5}$ to be uncertain by a factor of 2 (table 4-2 in JPL-2011 (Sander et al., 2011)).

Figure 3 displays the actinic spectrum relevant for the photolysis of N_2O_5 at stratospheric conditions. It shows that two distinct wavelength regions are important for the photolysis of N_2O_5, the region w_1 (200 - 258 nm) and the region w_2 (260 - 420 nm). While $\sigma_{N_2O_5}(\lambda,T)$ decreases over the whole wavelength region, the actinic flux modulates the actinic spectrum, mainly due to the absorption by O_2 and O_3. The minimum between the two maxima is caused by the combined effects of the O_3 absorption in the Hartley band, and the O_2 absorption in the Herzberg band. Thus, overhead O_2 and O_3 are crucial for the photolysis of N_2O_5 in the UV-C. The relative importance of each maximum depends on altitude and SZA. Therefore, if overhead ozone and total air mass is held fixed, observations at different altitudes and SZAs may provide independent information on the contribution of each wavelength region to $J_{N_2O_5}$. Noteworthy is also that in the wavelength range w_1, $\sigma_{N_2O_5}(\lambda,T)$ is temperature-independent and in w_2 temperature-dependent (Figure 2).

The temporal evolution of the NO_y species is modelled on 11 height levels (located between 655 K potential temperature (25.5 km) and 1099 K (35.5 km)) using the 1-D chemistry model LABMOS, which is an updated version of the model used by Bösch et al. (2003). It includes all relevant photochemical reactions of oxygen, nitrogen, hydrogen, chlorine, and bromine species according to kinetic and thermochemical data compiled in Sander et al. (2011). The model was integrated for 10 days using the commercial Facsimile software (). All modelled data shown are taken from the 10th day of the respective model run, in order to allow for spin-up of the NO_y partitioning.

The model is initialised for most species using the output of SLIMCAT simulations (Chipperfield, 2006) (run-id 336) for 5° N, 43° E for 2:00 LT on 17 June, 2005, except for NO_y species and O_3. For initialisation of the NO_y species HNO_3, N_2O_5, $ClONO_2$, HO_2NO_2, and $BrONO_2$, the measurements of the MIPAS-B (Michelson Interferometer for Passive Atmospheric Sounding-Balloon) instrument are taken, which were recorded 17 days prior to the mini-DOAS NO_2 measurements (e.g., Wetzel et al. (2002) and unpublished data). The model is further constrained by ozone measured by solar occultation measurements taken from the LPMA/DOAS payload (Limb Profile Monitor of the Atmosphere/Differential Optical Absorption Spectroscopy) 13 days prior to the NO_2 measurements.

Small mismatches in measured and modelled total NO_y are again removed by re-normalisation with the factor (nf) of the concentrations (NO_y) of the different NO_y species (Wiegele et al., 2009):

$$nf = NO_{y,MIPAS-B}/NO_{y,SLIMCAT}, \quad (3)$$

such that the NO_y partitioning given by SLIMCAT is preserved, but the total amount is constrained to the NO_y measured by the MIPAS-B instrument. Depending on the altitude, the normalisation factor ranges between 1 and 1.2. Figure 1 provides an overview on how the different NO_y species contribute to daytime NO_x production at different altitudes. Here the lower boundary of the striped area denotes the temporal evolution of the particular gas, and the striped area shows the total amount of NO_x, which is released by photolysis from the considered NO_y species. The dominant role of N_2O_5 destruction (red) for NO_x formation by R11, and R12 in the tropical mid-stratosphere at daytime is evident. In contrast all the other NO_y species including HNO_3 contribute to less than 10% to the NO_x increase during daytime.

2.3 Retrieval of $\sigma_{N_2O_5}(\lambda,T)$

If the model was complete (i.e. there was no missing chemistry), a comparison of measurements and model should provide information about the accuracy of the model and its components. We refer to the model output as NO_{2calc}, and the measured NO_2 as NO_{2meas}. However, 'calculated' concentrations are not totally independent from the measurements, since O_3 is relevant for the calculation of the actinic fluxes (see Section 2.2) and the partitioning of NO_y contributes to NO_{2calc}. Figure 4 shows NO_{2calc} and NO_{2meas} in the upper and lower panel, respectively. In the following we describe how the parameters s_1 and s_2 are retrieved from the measured and modelled field of NO_2. They are defined by

$$s_1 \cdot \sigma_{N_2O_5}(200-258nm)_{lab} = \sigma_{N_2O_5}(200-258nm)_{ret} \quad (4)$$

$$s_2 \cdot \sigma_{N_2O_5}(260-350nm)_{lab} = \sigma_{N_2O_5}(260-350nm)_{ret} \quad (5)$$

where the subscripts *lab* and *ret* and denote the laboratory measured and retrieved $\sigma_{N_2O_5}$, respectively. The measurement vector $\boldsymbol{y}$ is given by the subsequently measured NO_2 concentrations for h_i and t_j (Section 2.1)

$$y_{i,j} = NO_2(h_i,t_j) \quad (6)$$

and the state $\boldsymbol{x}$ is defined by the scaling factors s_1 and s_2.

$$x_k = s_k \quad (7)$$

The sensitivity of the NO_2 field to s_1 and s_2 can be quantitatively expressed by a weighting function or Jacobian matrix of derivatives of $[NO_2]_{i,j}$ with respect to the parameters s_1 and s_2, i.e., $\partial[NO_2]_{i,j}/\partial s_k$. For a given NO_2 profile with the indices i for a given altitude h_i and j for a given time t_j (Figure 5), the Jacobian with respect to s_1 and s_2 reads

$$K_{i,j,k} = \frac{\partial y_{i,j}}{\partial x_k}, \tag{8}$$

The forward model $\boldsymbol{F(x) = y}$ is constructed from the photochemical model as described in Section 2.2

The inferred sensitivity (i.e., Jacobians $K_{i,j,k}$) for s_1 and s_2 is shown in Figure 5. For s_1 it is a factor of 6 lower than for s_2, but both peak around 28 to 35 km altitude, i.e., where the measurements are taken. The maximum sensitivity ($\partial[NO_2]_{i,j}/\partial s_k$) is more extended in time for s_2 than for s_1, since in the UV-C (w_1) the spectral actinic flux is more dependent on SZA as compared to the UV-B/A wavelength range (w_2). Furthermore $\partial[NO_2]_{i,j}/\partial s_1$ peaks at higher altitudes as compared to $\partial[NO_2]_{i,j}/\partial s_2$, since attenuation in the UV-C occurs at smaller overhead air masses as compared to the UV-B/A wavelength range. For the purpose of a retrieval of s_1 and s_2 the matrix with elements $y_{i,j}$ is transformed into a 1-dimensional vector $\boldsymbol{y}$, that contains the NO_2 profiles for subsequent time steps t_j. Similarly, the kernel $K_{i,j,k}$ is transformed into a 2-dimensional matrix $\mathbf{K}$. In order to provide enough information on the state and to make the inversion mathematically feasible we need an additional constraint. Since an a priori $\boldsymbol{x_a}$ and a priori covariance (it's error matrix) is available and well defined through the JPL recommendations, we chose the optimal estimation technique (Rodgers, 2000) to estimate s_1 and s_2. Here, the retrieved state $\hat{\boldsymbol{x}}$ is constructed from both, prior information and the measurements, each weighted by the covariances $\mathbf{S}_\mathrm{a}$ and $\mathbf{S}_\epsilon$, respectively. Adopting the JPL recommendations as priori constraints, the a priori scaling factors s_k are unity and the associated a priori covariance matrix is diagonal with values of 2 in the diagonal.

The relationship between measurement and state is examined by the cost function defined by

$$\begin{aligned} \chi^2 = (\hat{\boldsymbol{x}} - \boldsymbol{x_a})\mathbf{S}_a^{-1}(\hat{\boldsymbol{x}} - \boldsymbol{x_a})^T \\ +(\boldsymbol{y_{mod}} - \boldsymbol{y_{meas}})\mathbf{S}_\epsilon^{-1}(\boldsymbol{y_{mod}} - \boldsymbol{y_{meas}})^T \end{aligned} \tag{9}$$

Since the measurement and the state do not linearly map, the state $\boldsymbol{x}$ is iteratively retrieved from (the subscript n now denotes the nth step)

$$\begin{aligned} \hat{\boldsymbol{x}}_{\boldsymbol{n+1}} = \boldsymbol{x_n} + (\mathbf{S_a}^{-1} + \mathbf{K_n}^T\mathbf{S}_\epsilon^{-1}\mathbf{K_n})^{-1} \\ \cdot[\mathbf{K_n}^T\mathbf{S}_\epsilon^{-1}(\boldsymbol{y} - F(\boldsymbol{x_n})) - \mathbf{S_a}^{-1}(\boldsymbol{x_n} - \boldsymbol{x_a})] \end{aligned} \tag{10}$$

where $\mathbf{K_n}$ is derived before each iteration for the current state $\boldsymbol{x_n}$. As the starting state we choose $\boldsymbol{x_0}$=$\boldsymbol{x_a}$. The diagonal elements of the measurement covariance $\mathbf{S}_\epsilon$ represent the squared error of the retrieved NO_2 measurements. For convergence criteria a certain step size from iteration n to n+1 is defined (Rodgers, 2000)

$$\sqrt{(\boldsymbol{x_{n+1}} - \boldsymbol{x_n})^2} \leq 0.04, \tag{11}$$

which is about one order of magnitude smaller than the expected noise error of the solution, as derived in Section 3.1.

3 Results and Discussion

Figure 6 shows χ^2 in the parameter space s_1 and s_2, where the minimum region (χ^2 = 30) is located at around s_1 = 1.2 to 2.6 and s_2= 0.7 to 1.1. After 10 iterations the global minimum is found at s_1 = 1.6 and s_2 = 0.9, i.e. our retrieval indicates a $\sigma_{N_2O_5}(\lambda,T)$ a factor 1.6 larger in the UV-C spectral range and a factor 0.9 smaller in the UV-B/A spectral range as compared to the recommended value in JPL-2011, with retrieval uncertainties of $\pm$0.80 and $\pm$0.26 for s_1 and s_2, respectively (see next section). Figure 6 shows the inferred result in the s_2/s_1 space together with their uncertainties, and the recommended JPL-2011 values. Figure 7 shows the resulting $\sigma_{N_2O_5}$.

Figure 4 shows the modelled (unscaled s_1 and s_2 in the upper panel, scaled s_1 and s_2 in the middle panel) and the measured diurnal NO_2 concentration (lower panel). Since there is still some discrepancy in the diurnal behaviour of the forward modelled state and the measurement, in the next section we investigate to what extent the errors and uncertainties of the measurement, as well as errors and uncertainties of the forward model, propagate into the inferred s_1 and s_2 values (see Table 1 for an overview on the errors and uncertainties).

3.1 Retrieval uncertainties

The measurement error ($\mathbf{S}_\mathrm{noise}$) of NO_2 has already been discussed by Kritten et al. (2010). According to Rodgers (2000), the propagation of the measurement noise into in the retrieval noise can be quantified by

$$\mathbf{S}_\mathrm{noise} = (\mathbf{K}^T\mathbf{S}_\epsilon^{-1}\mathbf{K})^{-1}. \tag{12}$$

which leads to 1-σ errors of $\pm$0.80 and $\pm$0.26 for s_1 and s_2, respectively.

3.2 Uncertainties in the forward model

We now discuss errors and uncertainties of s_1 and s_2 due to uncertainties in the forward model parameters, which are input parameters that influence the state but are not retrieved (Rodgers, 2000). Since the model is not linear in the forward model parameters, additional local retrievals of s_1 and s_2 at both the lower and upper boundary of the uncertainty range of these parameters are required. The difference in the retrieved s_1 and s_2 compared to the undisturbed case is taken as a measure for the uncertainty. The uncertainties are

not symmetrical, hence in each case an upper and a lower range of uncertainty is given. The forward model parameters in this study are input parameters to the chemical model. Among the many input parameters (i.e. model initialisation parameters as well as kinetic and thermochemical data), only those parameters which arguably exert the most influence on the results are considered. For model initialisation, these are total NO_y and O_3, and the absorption cross-section of NO_2. We also discuss the uncertainty in the actinic flux going into the calculation of $J_{N_2O_5}$. The following results are obtained:

(1) Initialisation of NO_y: As outlined above (section 2.2), the total amount of NO_y is initialised from MIPAS-B measurements. The accuracy of the MIPAS-B NO_y measurements above 20 km ranges between 4 and 7%. When initialising the model with NO_y at the lower boundary of the uncertainty range, the retrieval gives s_1 = 2.1 and s_2 = 1.0. When initialising the model with NO_y at the upper boundary of the uncertainty range, the retrieval gives s_1 = 1.3 and s_2 = 0.7. Accordingly the uncertainties due to initialisation of NO_y are Δs_1 = +0.5/-0.3 and Δs_2 = +0.1/-0.2.

(2) Initialisation of O_3: As outlined above (section 2.2), the O_3 profile is initialised from direct sun DOAS observations. The accuracy of these measurements above 20 km ranges between 5 and 29%. When initialising the model with O_3 at the lower boundary of the uncertainty range, the retrieval gives s_1 = 1.3 and s_2 = 0.7. When initialising the model with O_3 at the upper boundary of the uncertainty range, the retrieval gives s_1 = 1.9 and s_2 = 1.2. Accordingly, the uncertainties due to initialisation of O_3 are Δs_1 = +0.3/-0.4 and Δs_2 = +0.3/-0.2.

(3) Absorption cross-section of NO_2 (see reaction R9): The combined uncertainty of the NO_2 absorption cross-section and the quantum yield is a factor of 1.2 (Sander et al., 2011). When calculating the photolysis rates of NO_2 at the lower boundary of the uncertainty range of $\sigma_{N_2O_5}(\lambda,T)$, the retrieval gives s_1 = 1.1 and s_2 = 0.6. When calculating the photolysis rates of NO_2 at the upper boundary of the uncertainty range of $\sigma_{NO_2}(\lambda,T)$, the retrieval gives s_1 = 2.2 and s_2 = 1.2. Accordingly the uncertainties due to $\sigma_{NO_2}(\lambda,T)$ are Δs_1 = +0.6/-0.6 and Δs_2 = +0.3/-0.3. Evidently, despite its relatively small uncertainty, uncertainties in $\sigma_{NO_2}(\lambda,T)$ directly propagate into the modelled NO_2 concentration.

(4) The rate constant k_{NO+O_3} (see reaction R1): The uncertainty of the rate constant k_{NO+O_3} is temperature-dependent (Sander et al., 2011) and varies at temperatures relevant for this study between a factor of 1.30 and 1.42. When implementing a rate constant k_{NO+O_3} at the lower boundary of the uncertainty range, the retrieval gives s_1 = 2.1 and s_2 = 1.5. When implementing a rate constant k_{NO+O_3} at the upper boundary of the uncertainty range, the retrieval gives s_1 = 0.7 and s_2 = 0.6. Accordingly, the uncertainties due to the rate constant k_{NO+O_3} are Δs_1 = +0.5/-0.9 and Δs_2 = +0.6/-0.3.

(5) Actinic flux and $J_{N_2O_5}$: Another uncertainty in the calculated photolysis rates is due to uncertainties of the calculated actinic flux. In the mid- and upper stratosphere, uncertainties of the actinic flux are primarily due to the contribution of the direct solar irradiance rather than the contribution of scattered radiation from above or even from below (due to the absorption of ozone below 315 nm) for the altitude of interest (e.g., Madronich et al. (1985), Madronich (1987) and Bösch et al. (2003)). Scattering from below by clouds is not considered, because we could find no evidence of coulds through a comparison of modelled and measured limb radiances. Therefore, we asume major uncertainties in the spectral actinic flux relevant for $J_{N_2O_5}$ are primarily due to (a) the solar activity-dependent irradiance being particularly variable in the UV-C and UV-B spectral ranges, (b) overhead ozone, and (c) overhead O_2.

(a) In the UV-C and UV-A/B spectral ranges the spectral irradiance is known to be largely correlated with the solar activity (Foukal et al., 2006). Our measurements were conducted during the declining phase of solar cycle 23 in June 2005 with total solar sunspot numbers being around 30 (i.e. about 25% of the maximum sunspot number of cycle 23 seen in 2001). Therefore, it is rather likely that the solar radiation in the UV-C and UV-A was not particularly elevated during our measurement (Foukal et al., 2006). Further, during balloon flights conducted in 1996 and 1997, we measured the actinic flux relevant for photolysis of NO_2 in a similar descending phase solar cycle 22. No significant departure of the measured and modelled actinic fluxes was found (Bösch et al., 2003). Also, during three balloon flights conducted in 2003 and 2004, we measured the spectral solar irradiance. For the 325 - 370 nm spectral range reasonable agreement was found between our irradiance and the measurements of SIM, SCIAMACHY, SOLSPEC and Modtran 3.7 (within $< 5\%$), indicating no abnormal increase in the spectral irradiance in the UV-A in 2003 and 2004 when the sunspot numbers were larger than in 2005 (Gurlit et al., 2005). In addition, recent solar irradiance measurements claim that from solar maximum to minimum, solar radiation in the extreme UV may decrease four to six times more than predicted by models (Haigh et al., 2010). Accordingly, we see no reason to assume that radiation in the UV-C was particularly elevated during our measurements, at least not in an amount to explain an increased s_1 value.

(b) Ozone in the mid- and upper stratosphere used to scale the actinic flux was measured on several occasions during the same campaign. For our simulation overhead ozone measured at high accuracy by solar occultation spectroscopy is used (e.g., Butz et al. (2006) and Dorf et al. (2008)).

(c) Further the total overhead airmass and thus O_2 is determined by in-situ measured pressures and temperatures, and any significant departure would have been detected through a curved rather than straight line in a Langley plot of measured slant column amount of ozone (or BrO) versus total air mass (e.g., see Figure 2 in Dorf et al. (2008)).

Finally, the impact of a potentially too coarse wavelength grid (1 nm) in calculation of $J_{N_2O_5}$ (equation 1) should be

very small because of the lack of differential structures in $\sigma_{N_2O_5}(\lambda,T)$ (Trentmann et al., 2003). In conclusion, the error in the calculated $J_{N_2O_5}$ due to uncertainties of the calculated actinic flux is assumed to be negligible.

The individual uncertainties and errors of our study on $\sigma_{N_2O_5}(\lambda,T)$ are summarised in Table 1. In order to estimate a total error, we added positive and negative deviations separately in quadrature, even though we are aware that a Monte Carlo estimation would be more adequate, we used this approximation due to high computational costs of a Monte Carlo approach. The individual noise and forward model parameter errors add to a total error of +1.26 to -1.44 for s_1 and +0.79 to -0.57 for s_2.

4 Implications

Now we relate our results concerning $\sigma_{N_2O_5}(\lambda,T)$ to earlier descrepancies of measured and modelled N_2O_5 in the stratosphere and assess possible implications on global ozone. Previous inter-comparisons of measured and modelled N_2O_5 in the stratosphere reveal the following:

(a) The studies of Brühl et al. (2007) and Funke et al. (2011) also addressed inter-comparisons of N_2O_5 measured by ENVISAT/MIPAS. In particular for the retrieval from the IMK/IAA (Institut für Meteorologie und Klimaforschung and Instituto de Astrofísica de Andalucía) Brühl et al. (2007), stated a problem to reproduce the observed nighttime partitioning between N_2O_5 and NO_2 in the middle stratosphere using the recommended set of reaction coefficients and photolysis data, while for the Halloween solar proton event in late October 2003, the inter-comparison of measurements and model resulted in much larger modeled than measured N_2O_5, except for the KASIMA model (Funke et al., 2011).

(b) At the same time, Wolff et al. (2008) stated a low bias (-0.25 ppb) of ACE-FTS N_2O_5 relative to the MIPAS IMK-IAA retrieval for the middle stratosphere around 30 km.

(c) Moreover, in a recent study, Wetzel et al. (2012) found slightly larger measured MIPAS-B N_2O_5 concentrations than those modelled by EMAC (ECHAM/MESSy Atmospheric Chemistry) (e.g., Jöckel et al. (2005)) for the mid-stratosphere (22 - 34 km) at high latitudes during mid winter, i.e. SZA $> 86°$.

More recent sensitivity studies using SLIMCAT (not shown) indicate that in order to reconcile modelled and measured N_2O_5 for the studies mentioned in (a), the N_2O_5 photolysis frequency would need to be increased by at least a factor 1.5 to 2 in the UV-B/A. However an increase in UV-B/A photolysis of N_2O_5 by a factor 1.5 to 2 would deteriorate the existing agreement between N_2O_5 concentrations measured by ACE-FTS and simulated by SLIMCAT for sunrise and sunset (finding b), but at the same time it would potentially increase the discrepancy found in the study of Wetzel et al. (2012). Finally, such an increase is not supported by the result of our study.

A possible increase of $\sigma_{N_2O_5}(\lambda,T)$ in the UV-C spectral range as indicated by the present study would not resolve the discrepancies found in (a), mainly since below 10 mbar the UV-C radiation rapidly contributes less and less to the N_2O_5 photolysis as the altitude becomes lower. At the same time, it may not modify finding (b), and at best it would only slightly improve the mismatch found in (c).

Therefore, it is rather likely that the mismatch of the ENVISAT/MIPAS N_2O_5 with the various model predictions is not due to an incorrect $\sigma_{N_2O_5}(\lambda,T)$ used in the models, but due to any other reason.

In order to assess the consequences of our finding on global ozone, sensitivity simulations for the modified $\sigma_{N_2O_5}(\lambda,T)$ were performed using the SLIMCAT 3-D CTM (e.g., Chipperfield (1999), and Chipperfield (2006)). The model was run at a horizontal resolution of $5.6° \times 5.6°$ with 32 levels between the surface and $\sim$60 km. The model was forced using European Centre for Medium-Range Weather Forecasts (ECMWF) ERA-Interim data and used the model's standard stratospheric chemistry scheme. A first run (run R) used JPL-2011 photochemical data. A second run (N) was identical to run R but used the scaled values for $\sigma_{N_2O_5}$ derived in this work. Run N was initialised from run R in July 2007 and integrated for 2 years. Output from 2008 was used for this exercise.

Figure 8 shows the percentage change in annual mean O_3, NO_2 and N_2O_5 between runs N and R for 2008, along with the O_3 change in September. N_2O_5 decreases above 30 km by up to 4% in the annual (24-hour) mean due to the increased photolysis at short wavelengths. Below 30 km (35 km near the poles) N_2O_5 increases by up to 5% due to the slower photolysis at longer wavelengths. The change in NO_2 shows an opposite pattern reflecting the changing partitioning between NO_x and N_2O_5. Overall, the impact of the change in $\sigma_{N_2O_5}$ on ozone is small. In the mid-stratosphere (30-35 km) the increased NO_x, which is the main sink of odd oxygen in this region, leads to an O_3 decrease of about 0.25% with the scaled $\sigma_{N_2O_5}$. Below 30 km the ozone response changes sign, consistent with the NO_x change, but it is still only around 0.25%. In September O_3 loss inside the polar vortex is suppressed slightly (-0.6% change).

5 Summary and Conclusion

For the first time the absorption cross-section of N_2O_5 $\sigma_{N_2O_5}(\lambda,T)$ is constrained from measurements of the diurnal increase in NO_2 in the tropical mid-stratosphere. It is found that in the UV-C (200 - 260 nm) $\sigma_{N2O5}(\lambda,T)$ may be larger by a factor of 1.6 ± 0.8, and in the UVB/A (260 - 350 nm) smaller by a factor of 0.9 ± 0.26 as compared to the JPL-2011 recommendations. Additional uncertainties of our study are due to uncertainties of the forward model parameters, which are estimated to be up to +0.6 to -0.9 in the UV-C and up to +0.6 to -0.3 in the UV-B/A. A total error is esti-

mated to be +1.26 to -1.44 in the UV-C and +0.79 to -0.57 in the UV-B/A. The outcome of our study could be improved if other NO_y species (e.g., by MIPAS-B) were simultaneously measured. This was unfortunately not possible in a second attempt to simultaneously operate the MIPAS-B and mini-DOAS instrument in a joint deployment over North-Estern Brazil 2008 due to technical constraints.

Overall, above 30 km N_2O_5 concentrations decrease by to 4% in the annual (24-hour) mean due to the increased photolysis at short wavelengths, when using the retrieved $\sigma_{N_2O_5}(\lambda,T)$. Below 30 km (35 km near the poles) N_2O_5 increases by up to 5% due to the slower photolysis at longer wavelengths. For this altitude region in some cases lower measured than modelled N_2O_5 have been reported for the late morning lower stratosphere (e.g., in yet unpublished comparison studies of SLIMCAT simulations with EMVISAT-MIPAS N_2O_5 measurements), which could be reconciled increasing $\sigma_{N_2O_5}(\lambda,T)$ in the UV-B/A wavelength range by up to a factor of 2 compared to the JPL-2011 recommendations (e.g., as indicated by recent SLIMCAT runs). Increasing the N_2O_5 photolysis in the UV-C according to our finding is not enough to eliminate the stated mismatch of measured and modelled N_2O_5 for altitudes above 30 km. Therefore firm conclusions on a larger UV-C N_2O_5 absorption cross section as indicated by our study can not be drawn from previous measurement versus model inter-comparison studies.

Further a sensitivity test using our revised versus the JPL-2011 recommended $\sigma_{N_2O_5}(\lambda,T)$ show little effects on global ozone. Above 30 km, where UV-C light is strongly contributing to the N_2O_5 photolysis, the increase in $\sigma_{N_2O_5}(\lambda,T)$ (1.6 ± 0.8 in the w_1 wavelength region), leads to an increase in NO_2 and through R2 to 0.2% less ozone at most. Below 30 km, where N_2O_5 photolysis due to UVB/A light is more important, our smaller $\sigma_{N_2O_5}(\lambda,T)$ (0.9 ± 0.26 in the w_2 wavelength region) leads to slightly more ozone, i.e. 0.2% in the mid-latitude stratosphere, and as much as 0.6% in the 20 - 25 km region over the Antartica in spring.

Finally our approach could also be used to retrieve more and other parameters from simultaneous atmospheric measurements of the relevant NO_y species, including a tighter assessment of the absorption cross-section of NO_2.

Acknowledgements. Funding for this study came from the Deutsche Forschungsgemeinschaft (DFG) (grants Pf 384/5-1/2, PF384/9-1/2), Deutsches Zentrum für Luft und Raumfahrt (DLR) (contracts BMWi 50EE0840), the European Union (EU) through the EU projects Reconcile (FP7-ENV-2008-1-226365), and SHIVA (FP7-ENV-2007-1-226224) and the European Space Agency (ESA) (contract (ESA-ESRIN: No. RFQ/3-12092/07/I- 435 OL). The SLIMCAT modelling was supported by the NERC National Centre for Atmospheric Science (NCAS), UK and we thank Wuhu Feng for his help. We thank the CNES equipe nacelles pointées and the balloon team from Aire sur l'Adour/France without which the balloon flight would not have been possible. We also thank our colleagues from the LPMA balloon team (P. Jeseck, I. Pepin and Y. Té) for the successful cooperation. Finally, we are grateful for the hospitality and support given by the personnel of the Instituto Nacional de Pesquisas Espaciais (INPE), Brazil to successfully perform the balloon flight at Teresina/Brazil. A. Butz is funded through the Emmy-Noether programme of the Deutsche Forschungsgemeinschaft (DFG) grant BU2599/1-1 (RemoteC).

References

Bösch, H., Camy-Peyret, C., Chipperfield, M. P., Fitzenberger, R., Harder, H., Platt, U., and Pfeilsticker, K.: Upper limits of stratospheric IO and OIO inferred from center-to-limb-darkening corrected balloon-borne solar occultation visible spectra: Implications for total gaseous iodine and stratospheric ozone, J. Geophys. Res., 108, 4455, doi:10.1029/2002JD003078, 2003.

Butz, A., Bösch, H., Camy-Peyret, C., Chipperfield, M., Dorf, M., Dufour, G., Grunow, K., Jeseck, P., Kühl, S., Payan, S., Pepin, I., Pukite, J., Rozanov, A., von Savigny, C., Sioris, C., Wagner, T., Weidner, F., and Pfeilsticker, K.: Inter-comparison of stratospheric O_3 and NO_2 abundances retrieved from balloon borne direct sun observations and Envisat/SCIAMACHY limb measurements, Atmos. Chem. Phys., 6, 1293–1314, 2006.

Brasseur, G. and Solomon, S.: Aeronomy of the middle atmosphere, Springer, P.O. Box 17, 3300 AADordrecht, The Netherlands, 2005.

Brühl, C. and Steil, B. and Stiller, G. and Funke, B. and Jöckel, P.: Nitrogen compounds and ozone in the stratosphere: comparison of MIPAS satellite data with the chemistry climate model ECHAM5/MESSy1, Atmos. Chem. Phys., 7, 5585-5598, doi:10.5194/acp-7-5585-2007, 2007.

Chipperfield, M. P.: Multiannual simulations with a three-dimensional chemical transport model, J. Geophys. Res., 104, 1781–1805, 1999.

Chipperfield, M. P.: New Version of the TOMCAT/SLIMCAT Off-Line Chemical Transport Model: Intercomparison of Stratospheric Tracer Experiments, Q. J. R. Meteorol. Soc., 132, 1179–1203, doi:10.1256/qj.05.51, 2006.

Crutzen, P. J.: The influence of nitrogen oxides on the atmospheric ozone content, Q. J. R. Meteorol. Soc. 96, 320, 1970.

Dorf, M., A. Butz, C. Camy-Peyret, M. P. Chipperfield, L. Kritten, and K. Pfeilsticker, Bromine in the tropical troposphere and stratosphere as derived from balloon-borne BrO observations, Atmos. Chem. Phys., 8, 7265–7271, 2008.

Deutschmann, T., S. Beirle, U. Frieß, M. Grzegorski, C. Kern, L. Kritten, U. Platt, C. Prados-Román, J. PukIite, T. Wagner, B. Werner, and K. Pfeilsticker: The Monte Carlo atmospheric radiative transfer model McArtim: Introduction and validation of Jacobians and 3D features, J. Quant. Spectrosc. Ra., 112, 1119–1137, ISSN 0022-4073, DOI: 10.1016/j.jqsrt.2010.12.009, 2011.

FACSIMILE software, MCPA Software Ltd., Oxfordshire, UK.

Foukal P., C. Fröhlich, H. Spruit, and T. M. L. Wigley: Variations in solar luminosity and their effect on the Earth's climate, Nature, 443, 161–166, doi:10.1038/nature05072, 2006.

Funke, B. and Baumgaertner, A. and Calisto, M. and Egorova, T. and Jackman, C. H. and Kieser, J. and Krivolutsky, A. and López-Puertas, M. and Marsh, D. R. and Reddmann, T. and Rozanov, E. and Salmi, S.-M. and Sinnhuber, M. and Stiller, G. P. and Verronen, P. T. and Versick, S. and von Clarmann, T. and Vyushkova, T. Y. and Wieters, N. and Wissing, J. M.: Composition changes

after the "Halloween" solar proton event: the High Energy Particle Precipitation in the Atmosphere (HEPPA) model versus MIPAS data intercomparison study, Atmos. Chem. Phys., 11, 9089-9139, doi:10.5194/acp-11-9089-2011, 2011.

Gebhardt, C., Rozanov, A., Hommel, R., Weber, M., Bovensmann, H., Burrows, J. P., Degenstein, D., Froidevaux, L., and Thompson, A. M.: Stratospheric ozone trends and variability as seen by SCIAMACHY during the last decade, Atmos. Chem. Phys. Discuss., 13, 11269-11313, doi:10.5194/acpd-13-11269-2013, 2013.

Gurlit, W., H. Bösch, H. Bovensmann, J. Burrows, A. Butz, C. Camy-Peyret, M. Dorf, K. Gerilowski, A. Lindner, S. Noel, U. Platt, F. Weidner, and K. Pfeilsticker: The UV-A and visible solar irradiance spectrum: Inter-comparison of absolutely calibrated, spectrally medium resolved solar irradiance spectra from balloon- and satellite-borne measurements, Atmos. Chem. Phys., 5, 1879–1890, 2005.

Haigh, J. D., Winning, A. R., Toumi, R., Harder, J. W.: An influence of solar spectral variations on radiative forcing of climate, Nature, 467, Issue 7316, doi:10.1038/nature09426, 2010.

Harwood, M. H., Jones, R. L., Cox, R. A., Lutman, E. and Rattigan, O. V.: Temperature-dependent absorption cross-sections of N_2O_5, J. Photochem. Photobiol. A:Chem., 73, 167–175, 1993.

Harwood, M. H., Burkholder, J. B. and Ravishankara, A. R.: Photodissociation of $BrONO_2$ and N_2O_5: Quantum Yields for NO_3 Production at 248, 308, and 352.5 nm, J. Phys. Chem. A, 102, 1309–1317, 1998.

IPCC, 2007: Climate Change 2007: The Physical Science Basis. Contribution of Working Group I to the Fourth Assessment Report of the Intergovernmental Panel on Climate Change [Solomon, S., D. Qin, M. Manning, Z. Chen, M. Marquis, K.B. Averyt, M.Tignor and H.L. Miller (eds.)]. Cambridge University Press, Cambridge, United Kingdom and New York, NY, USA.

Jöckel, P., Sander, R., Kerkweg, A., Tost, H., and Lelieveld, J.: Technical Note: The Modular Earth Submodel System (MESSy) a new approach towards Earth System Modeling, Atmos. Chem.Phys., 5, 433444, doi:10.5194/acp-5-433-2005, 2005.

Johnston, H. S.: Reduction of stratospheric ozone by nitrogen oxide catalysts from supersonic transport exhaust. Science, 173, 517–522, 1971.

Jones E. J. and Wulf O. I.: The absorption coefficient of nitrogen pentoxide in the ultraviolet and the visible absorption spectrum of NO_3, J. Chem. Phys. 5, 873–877, 1937.

Kritten, L., Butz, A., Dorf, M., Deutschmann, T., Kühl, S., Prados-Roman, C., Pute, J., Rozanov, A., Schofield, R., and Pfeilsticker, K.: Time dependent profile retrieval of UV/vis absorbing radicals from balloon-borne limb measurements: a case study on NO_2 and O_3, Atmos. Meas. Tech., 3, 933–946, doi:10.5194/amt-3-933-2010, 2010.

Kreycy, S., Camy-Peyret, C., Chipperfield, M. P., Dorf, M., Feng, W., Hossaini, R., Kritten, L., Werner, B., and Pfeilsticker, K.: Atmospheric test of the J(BrONO2)/kBrO+NO2 ratio: implications for total stratospheric Bry and bromine-mediated ozone loss, Atmos. Chem. Phys., 13, 6263-6274, doi:10.5194/acp-13-6263-2013, 2013.

Lary, D. J. and Pyle, J. A.: Diffusive radiation, twilight and photochemistry, J. Atmos. Chem., 13, 373–392, 1991.

Madronich, S., D. R. Hastie, H. I. Schiff, and B. A. Ridley, Measurements of the photodissociation coefficient of NO2 in the atmosphere, II. Stratospheric measurements, J. Atmos. Chem., 3, 233-245, 1985.

Madronich, S., Photodissociation in the atmosphere 1. Actinic flux and the effects of ground reflections and clouds, J. Geophys. Res., 92, 9740-9752, 1987.

Oh, D., W. Sisk, A. Young and H. Johnston, J.: Nitrogen Dioxide Flourescence from N_2O_5 Photolysis, Chem. Phys., 85, 7146–7158, 1986.

Osborne, B. A., Marston, G., Kaminski, L., Jones, N. C., Gingell, J. M., Mason, N. J., Walker, I. C., Delwiche, J. and Hubin-Franskin, M.-J.: Vacuum ultraviolet spectrum of dinitrogen pentoxide, J. Quant. Spectrosc. Radiat. Transfer, 64, 67–74, 2000.

Park, S., P. Croteau, K. A. Boering, D. M. Etheridge, D. Ferretti, P. J. Fraser, K-R. Kim, P. B. Krummel, R. L. Langenfelds,T. D. van Ommen,L. P. Steele, and C. M. Trudinger: Trends and seasonal cycles in the isotopic composition of nitrous oxide since 1940, Nature Geoscience, 5, 261 - 265, doi:10.1038/ngeo1421, (2012).

Platt, U. and Stutz, J.: Differential Optical Absorption Spectroscopy (DOAS), Principle and Applications, Springer Verlag, Heidelberg, 2008.

Ravishankara, A. R., Daniel, J. S., and Portmann, R. W.: Nitrous Oxide (N_2O): The Dominant Ozone-Depleting Substance Emitted in the 21st Century, Science, 326, 123–125, 2009.

Rodgers, C. D.: Inverse methods for atmospheric sounding, World Scientific, Singapore, New Jersey, London, Hongkong, 2000.

Sander, S., Friedl, R. R., Barkern, J., Golden, D., Kurylo, M., Wine, P., Abbat, J., Burkholder, J., Moortgart, C., Huie, R., and Orkin, R. E.: Chemical kinetics and photochemical data for use in atmospheric studies, Technical Report, NASA/JPL Publication, 17, 2011.

Trentmann, J., Bovensmann, H., Eyring, V., Mueller, R., Burrows, J.P.: Impact of Accurate Photolysis Calculations on the Simulation of Stratospheric Chemistry, J. Atmos. Chem., 44, 225–240, 2003.

Weidner, F., Bösch, H., Bovensmann, H., Burrows, J. P., Butz, A., Camy-Peyret, C., Dorf, M., Gerilowski, K., Gurlit, W., Platt, U., von Friedeburg, C., Wagner, T., and Pfeilsticker, K.: Balloon-borne Limb profiling of UV/vis skylight radiances, O_3, NO_2, and BrO: Technical set-up and validation of the method, Atmos. Chem. Phys., 5, 1409–1422, 2005.

Wetzel, G., Oelhaf, H., Ruhnke, R., Friedl-Vallon, F., Kleinert, A., Kouker, W., Maucher, G., Reddmann, T., Seefeldner, M., Stowasser, M., Trieschmann, O., von Clarmann, T. and Fischer, H.: NOy partitioning and budget and its correlation with N2O in the Arctic vortex and in summer mid-latitudes in 1997, J. Geophys. Res., 107, 4280, doi:10.1029/2001JD000916, 2002.

Wetzel, G., Oelhaf, H., Kirner, O., Friedl-Vallon, F., Ruhnke, R., Ebersoldt, A., Kleinert, A., Maucher, G., Nordmeyer, H., and Orphal, J.: Diurnal variations of reactive chlorine and nitrogen oxides observed by MIPAS-B inside the January 2010 Arctic vortex, Atmos. Chem. Phys., 12, 6581-6592, doi:10.5194/acp-12-6581-2012, 2012.

Wiegele, A., Kleinert, A., Oelhaf, H., Ruhnke, R., Wetzel, G., Friedl-Vallon, F., Lengel, A., Maucher, G., Nordmeyer, H., and Fischer, H.: Spatio-temporal variations of NOy species in the northern latitudes stratosphere measured with the balloon-borne MIPAS instrument, Atmos. Chem. Phys., 9, 1151–1163, doi:10.5194/acp-9-1151-2009, 2009.

WMO (World Meteorological Organization), Scientific Assessment of Ozone Depletion: 2010, Global Ozone Research and Monitoring Project-Report No. 52, 516 pp., Geneva, Switzerland, 2011.

WMO (World Meteorological Organization), Press Release No. 934, 2013.

Wolff, M. A. and Kerzenmacher, T. and Strong, K. and Walker, K. A. and Toohey, M. and Dupuy, E. and Bernath, P. F. and Boone, C. D. and Brohede, S. and Catoire, V. and von Clarmann, T. and Coffey, M. and Daffer, W. H. and De Mazière, M. and Duchatelet, P. and Glatthor, N. and Griffith, D. W. T. and Hannigan, J. and Hase, F. and Höpfner, M. and Huret, N. and Jones, N. and Jucks, K. and Kagawa, A. and Kasai, Y. and Kramer, I. and Küllmann, H. and Kuttippurath, J. and Mahieu, E. and Manney, G. and McElroy, C. T. and McLinden, C. and Mébarki, Y. and Mikuteit, S. and Murtagh, D. and Piccolo, C. and Raspollini, P. and Ridolfi, M. and Ruhnke, R. and Santee, M. and Senten, C. and Smale, D. and Tétard, C. and Urban, J. and Wood, S.: Validation of HNO_3, $ClONO_2$, and N_2O_5 from the Atmospheric Chemistry Experiment Fourier Transform Spectrometer (ACE-FTS), Atmos. Chem. Phys., 8, 3529-3562, doi:10.5194/acp-8-3529-2008, 2008.

Yao, F., Wilson, I., and Johnston, H.: Temperature-dependent ultraviolet absorption spectrum for dinitrogen pentoxide, J. Phys. Chem., 86, 3611–3615, 1982.

Table 1. Uncertainties in the retrieval of s_1 and s_2.

	Retrieved Value	Noise	NO_y Initialisation	O_3 Initialisation	σ_{NO_2}	k_{NO+O_3}	total
s_1	1.6	±0.80	+0.5,-0.3	+0.3,-0.40	+0.5,-0.6	+0.6,-0.9	+1.26,-1.44
s_2	0.9	±0.26	+0.1,-0.2	+0.3,-0.2	+0.3,-0.3	+0.6,-0.3	+0.79,-0.57

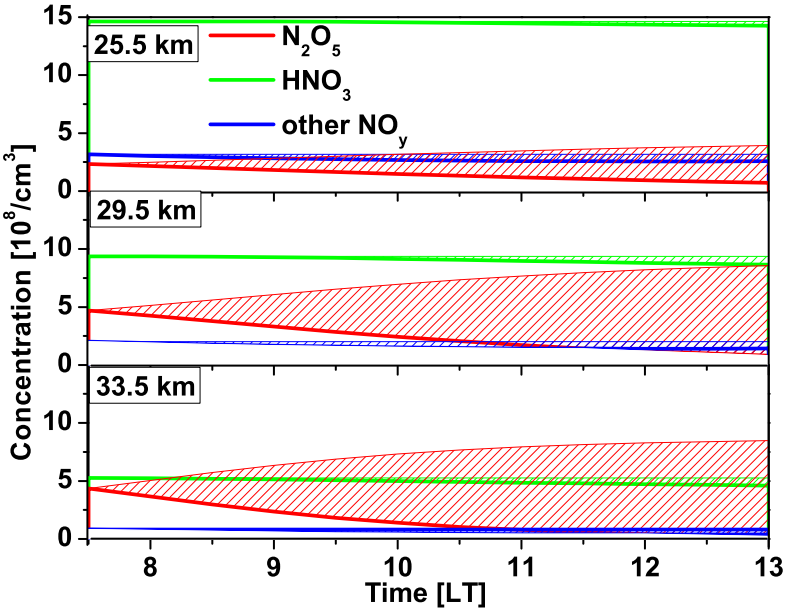

Fig. 1. Temporal evolution of N_2O_5 (red), HNO_3 (green) and the sum of other NO_y species ($ClONO_2$ + HO_2NO_2 + $BrONO_2$, blue) for different altitudes of the tropical mid-stratosphere (5.1° S, 43.6° W). The lower boundary of the striped area denotes the temporal evolution of the particular gas, and the striped area shows the total amount of NO_x, which is released by photolysis from the considered NO_y species. Note that the release from N_2O_5 is double due to two N atoms.

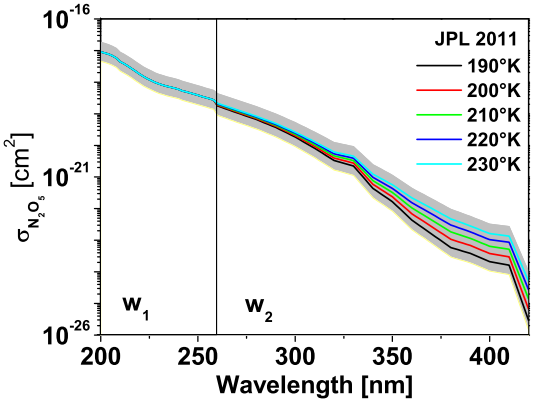

Fig. 2. Absorption cross-section and uncertainty of $\sigma_{N2O5}(\lambda,T)$ as recommended by JPL 2011 (Sander et al., 2011) (yellow area). For this study, $\sigma_{N2O5}(\lambda,T)$ is divided into two wavelength regions w_1 and w_2. No temperature dependence of $\sigma_{N2O5}(\lambda,T)$ is reported for w_1, the T dependence for w_2 is indicated by different colours.

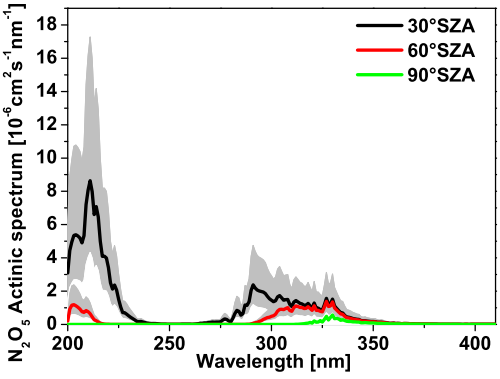

Fig. 3. Actinic spectrum of N_2O_5 (i.e., the product of $\sigma_{N2O5}(\lambda,T)$ (at 230 K) and modelled actinic fluxes) for an overhead ozone column of 283 Dobson Units, and different SZAs at 30.5 km.

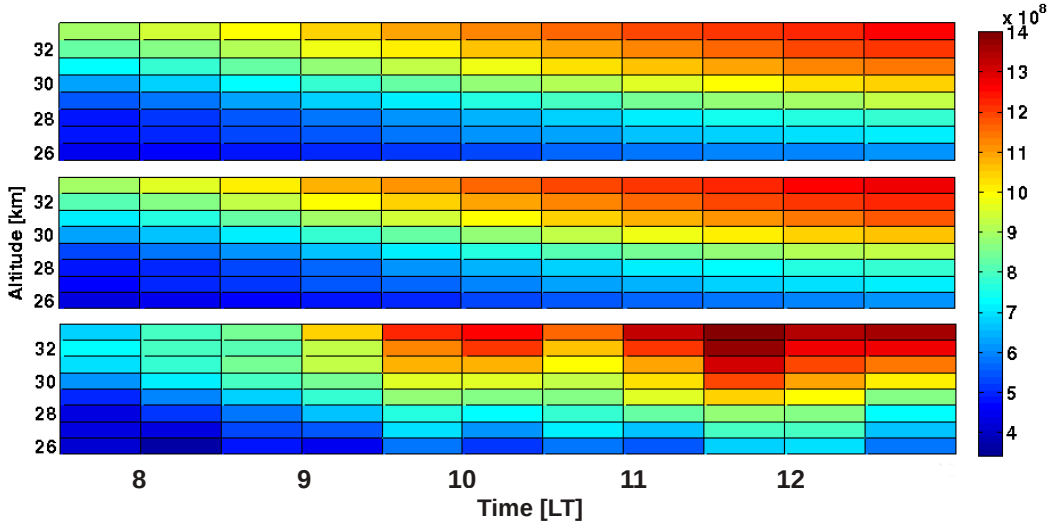

Fig. 4. Temporal evolution of the NO_2 concentration in the tropical mid-stratosphere (5.1° S, 43.6° W) for June 13, 2005, using the JPL-2011 recommendation for $\sigma_{N2O5}(\lambda,T)$ i.e., s_1 = 1.0 and s_2 = 1.0 (upper panel). Middle panel: Same as in the upper panel, but with the inferred s_1 = 1.6 and s_2 = 0.9 (middle panel). Lower panel: Measured NO_2. Units are given in $\mathrm{molec/cm^3}$.

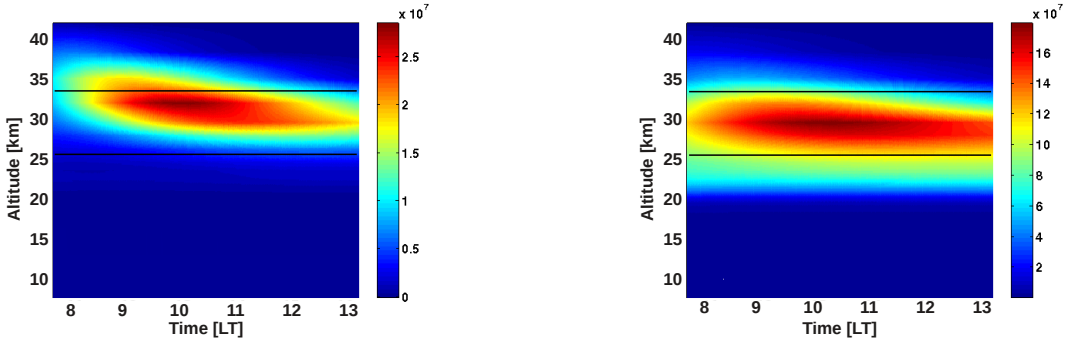

Fig. 5. Sensitivity of the NO_2 concentration in our model to the scaling factors s_1 (left panel) and s_2 (right panel) on the absorption cross-section of N_2O_5. Units are given in 10^7 $\mathrm{molec/cm^3}$. The altitude region used for the analysis is marked by black lines.

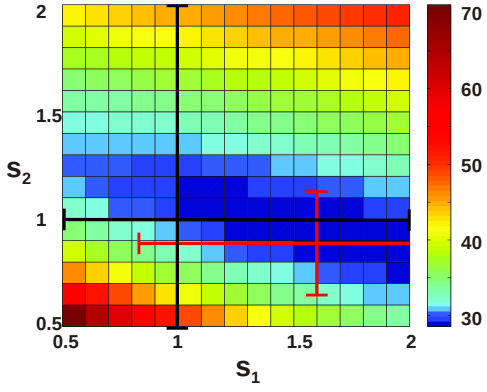

Fig. 6. χ^2 as a function of s_1 and s_2, as given in Eq. (9). The inferred global minimum is shown in red together with the total error due to noise error of the retrieval. The corresponding JPL-2011 values are given in black.

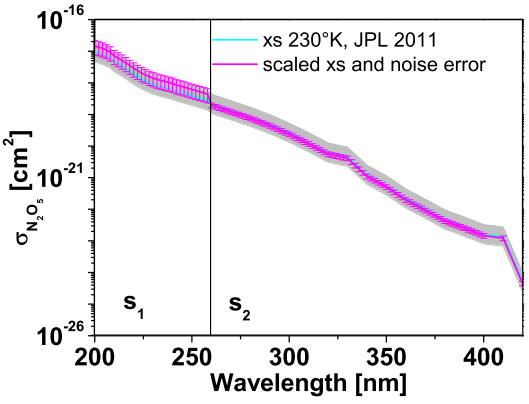

Fig. 7. $\sigma_{N2O5}(\lambda,T)$ measured in the laboratory (JPL-2011, shown in light blue) and inferred in the present study (shown in pink).

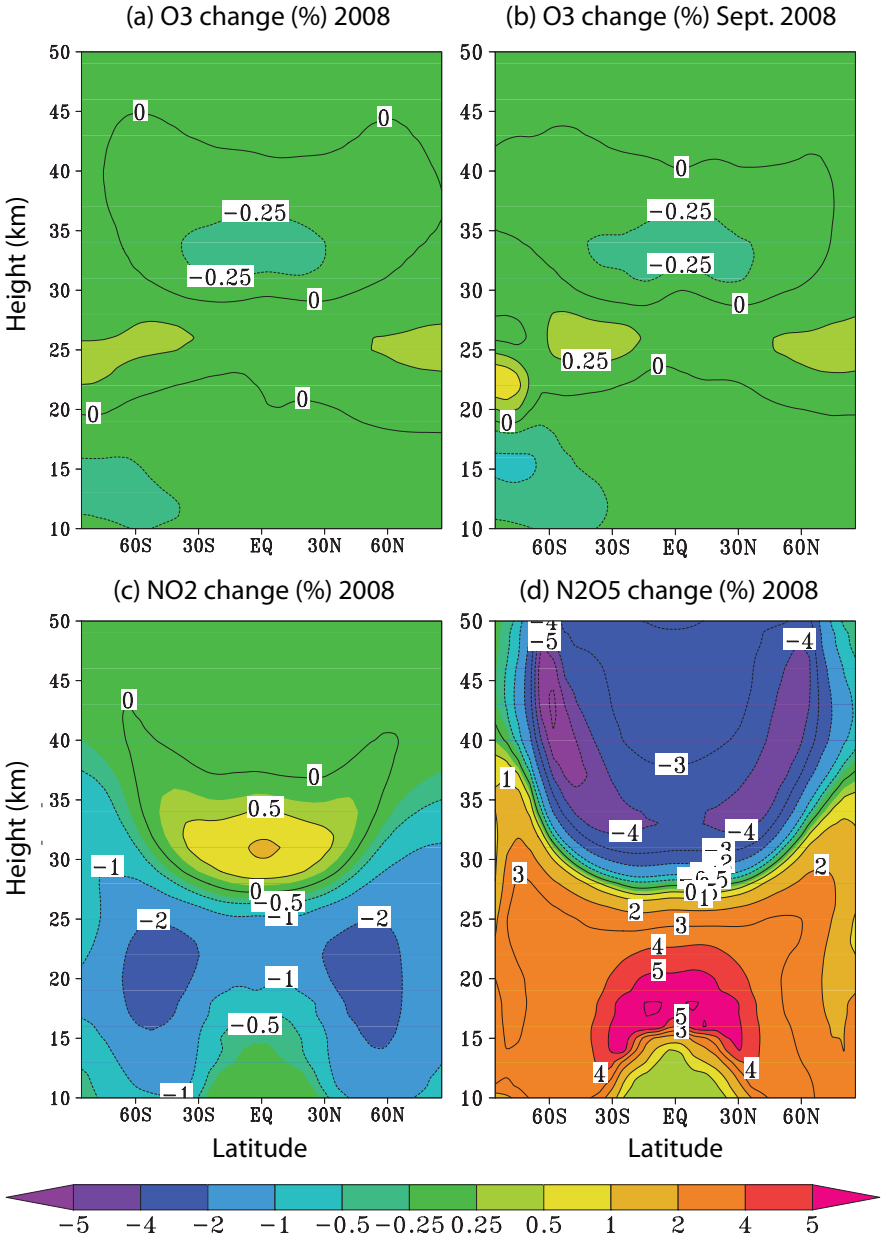

Fig. 8. Difference in zonal mean fields (%) for 2008 from the run of the SLIMCAT 3-D CTM with scaled $J_{N_2O_5}$ (run N) minus the run with recommended JPL-2011 kinetics (run R) for (a) annual mean O_3, (b) September mean O_3, (c) annual mean NO_2, and (d) annual mean N_2O_5. Note irregular contour interval.